Construction and Building Materials 458 (2025) 139514

Contents lists available at ScienceDirect

Construction and Building Materials

journal homepage: www.elsevier.com/locate/conbuildmat

Strength distribution predictions of glued laminated timber beams: Influence of size, load configuration, and strength class described by the finite weakest-link theory

Christoffer Vida *, Markus Lukacevic, Sebastian Pech, Josef Füssl

Institute for Mechanics of Materials and Structures, TU Wien, Karlsplatz 13/202, 1040 Vienna, Austria

ARTICLE INFO

Keywords:
Size effect
Quasi-brittle material
Glued laminated timber
Probability distribution
Structural reliability
Finite weakest-link theory

ABSTRACT

In structural engineering, assessing the probability of failure is crucial for reliability considerations in design codes. Most experimental studies on glued laminated timber (GLT) beams have focused on small-scale beams, leaving a gap in understanding the failure probabilities of large-scale structures up to 3 m. Despite the use of various probability distribution functions (PDFs) to characterize GLT beam strength, a comprehensive mechanics-based approach that accounts for beam size, load configurations, and strength classes remains absent. To address this, we applied the finite weakest-link theory to model the PDFs of GLT beams with homogeneous layup according to European standards. This study details the parameter identification process, compares model predictions with experimental data, explores trends for large-scale beams, and discusses the implications for structural reliability.

Our model predictions showed strong agreement with data from nine experimental studies involving 556 beams. For large-scale beams, where no experimental data was available, the predicted trends aligned with an independent numerical study. The characteristic bending and tensile strengths were successfully modeled in accordance with European standards, and an exemplary structural reliability analysis revealed diverging trends when comparing the Weibull-Gaussian distribution with the commonly used log-normal distribution. In conclusion, this statistical mechanics-based model effectively characterizes the PDFs of homogeneous GLT beams based on size, load configuration, and strength class. The left tail of strength distributions is essential for assessing structural reliability. While this tail has been characterized through simulations, detailed experimental investigations will be required to validate these findings.

1. Introduction

Stochastic knowledge of material properties is crucial for formulating holistic design concepts, particularly in timber engineering. Wood, due to its natural growth process, exhibits higher variability compared to other building materials like steel, concrete, or brick. Timber constructions have seen a rise in both number and size in recent years. The size limitations of individual wooden boards can be overcome by manufacturing glued laminated timber (GLT) beams, achieved by gluing finger-jointed boards on top of each other. This manufacturing process also results in the homogenization of material properties. The dimensions of these beams vary in practical applications, with depths reaching up to 3 m.

The variation of strength can be described by probability distribution functions (PDFs). Various distribution types have been used in experimental studies [1–10] to characterize the bending strength of GLT beams, such as the normal (Gaussian) distribution in [1], the log-normal distribution in [5], and the three-parameter Weibull distribution in [3]. Typically, the obtained PDFs correspond to only a single set of experimental data with the same test configuration. A theoretical framework is desirable that provides the strength distribution depending on the strength class, load configuration, and beam size:

- The *strength class* ensures that a product meets specific characteristics such as strength, stiffness, and density. While prEN 1995-1-1 [11] provides the design concept of GLT beams, EN 14080 [12] defines the strength grade for the boards, the strength of finger-joints, and the overall beam layup. For instance, the 5th-percentile bending strength depends on the strength class. Thus, the resistance level of a structure is also determined by this strength class.

* Corresponding author.
E-mail addresses: christoffer.vida@tuwien.ac.at (C. Vida), markus.lukacevic@tuwien.ac.at (M. Lukacevic), sebastian.pech@tuwien.ac.at (S. Pech), josef.fuessl@tuwien.ac.at (J. Füssl).

https://doi.org/10.1016/j.conbuildmat.2024.139514
Received 30 August 2024; Received in revised form 22 October 2024; Accepted 7 December 2024

- In timber engineering, load configurations often lead to a combination of tensile and bending stress states. Nevertheless, pure tensile and bending strength are typically distinguished to align with experimental observations, e.g., in [3,6]. From a continuum mechanics perspective, this distinction can be misleading. For instance, the same tensile stress acting on a material point can be caused by either tensile or bending load configurations. The behavior of the material point is driven only by the acting stresses, independent of their cause. Thus, the distinguished tensile and bending strengths are not material strengths but rather structural properties depending on the load configuration.
- The effect of *beam size* on bending strength is typically recognized in design codes, e.g., with the depth modification factor in prEN 1995-1-1 [11]. Multiple studies have focused on determining the size effect experimentally, e.g., in [4,6]. However, large-scale testing of GLT beams involves a tremendous effort. Thus, for large beams, the so-called size effect has been studied with numerical simulations, e.g., in [13–15]. These studies found differing trends for the 5th-percentile bending strength with varying beam sizes but revealed that with increasing beam size, the coefficient of variation (CV) of the bending strength decreases. Recently, Fink et al. [16] confirmed that the CV is likely to decrease for large beams by compiling results from numerous experimental studies in the literature.

Such a flexible theoretical framework enables the effective assessment of structural reliability for GLT beams in various scenarios. This is essential for developing design concepts that maintain constant reliability, despite the diverse demands faced by modern structures.

1.1. Theoretical frameworks and structural reliability

A widely used framework for describing the change in strength PDFs of timber is Weibull's statistical strength theory [17], which conceptually defines the tensile strength by the weakest link in a chain. The theory derives the Weibull distribution for isotropic brittle materials, allowing scaling based on stress distribution and volume. Bohannan [18] applied the theory to describe the size effect of GLT beams subjected to bending. While the theory explains the strength decrease with increasing stressed volume, it maintains a constant CV independent of the scaling.

Schilling et al. [19] proposed adjusting both parameters of the two-parameter Weibull distribution based on beam depth. While this approach results in decreasing strength and CV, it contradicts the use of material-related parameters for the distribution, as originally intended by Bohannan [18]. The adjustments were derived from numerical simulations of beams in four-point bending, with depths ranging from $0.3\,\mathrm{m}$ to $3.0\,\mathrm{m}$ and a fixed length-to-depth ratio [14].

These approaches are only partially effective. Weibull's statistical strength theory is inadequate because wood failure is quasi-brittle rather than brittle. Failure in quasi-brittle materials is influenced by a fracture process zone ahead of the crack tip, which is significant in size relative to the cross-section dimensions and enables stress redistribution [20]. Moreover, implementing a decreasing CV requires violating the assumption of constant, material-related parameters.

Bažant and Pang [21,22] proposed a statistical mechanics-based framework to characterize tensile or bending strength PDFs of quasi-brittle materials. The framework uses a Weibull-Gaussian distribution, combining a Weibull part for the left tail with a Gaussian part for the remainder. Conceptually, it accounts for stress distribution and volume by forming a chain of finite elements, within which stress redistribution is possible. Ultimate failure occurs when a single element collapses. This so-called finite weakest-link theory has proven successful for various quasi-brittle materials such as ceramics [23], asphalt [24], and oak boards [25]. Recently, Tapia and Aicher [26] applied the theory to glued laminated timber made of oak boards.

An accurate strength distribution is essential for structural reliability assessments, as it characterizes the resistance. Commonly, the strength of timber structures is assumed to follow a log-normal distribution, as in EN 14358 [27] and JCSS [28]. For bending strength distributions of GLT beams, JCSS [28] recommends a CV of 0.15, independent of their size. So, there exists a significant knowledge gap in comprehensively describing the strength distribution of GLT beams influenced by their size, load configuration, and strength class. It is expected that the depending characteristics of the distribution influence the structural reliability. Addressing this gap is essential for developing holistic design concepts that aim for constant reliability of structures regardless of their size.

1.2. Scope of this work

To address this knowledge gap, we identified five key parameters for GLT beams that define the grafted Weibull-Gaussian distribution within the finite weakest-link theory. Our focus is on GLT beams made of softwoods with a homogeneous layup, meaning the individual boards belong to the same strength class. The initial parameters were derived from a comprehensive numerical simulation study [15]. Subsequently, one parameter was refined based on an experimental study [3], while another was adjusted to align the distribution with European strength classes [12]. This statistical mechanics-based model enabled the prediction of trends in decreasing mean strength and CV across different beam sizes, including large beams up to $3\,\mathrm{m}$ in depth. A structural reliability analysis followed, aiming to achieve consistent structural reliability using Weibull-Gaussian or log-normal distributions.

This paper is organized as follows: Section 2 covers the fundamentals of the finite weakest-link theory, presents the model parameters and fitting procedure, and compiles experimental and numerical results. In Section 3, the fitting of the model parameters is shown, which are further used in Sections 4 and 5. This is followed by a comparison of predicted mean strengths and their CVs with experimental data, and an in-depth discussion of the model parameters. Section 4 provides predicted trends for large GLT beams and explores the influence of size and load configuration on the PDFs. Section 5 demonstrates the model's implications through an exemplary structural reliability analysis. It explores how constant reliability is maintained when using either a Weibull-Gaussian or log-normal distribution, and includes a sensitivity analysis of one key parameter of the Weibull-Gaussian distribution. The paper concludes with a summary of the model parameters and their derivation, the conclusions, and an outlook discussing further necessary research and potential extensions (Section 6).

2. Materials and methods

The finite weakest-link theory [21,22,29] offers a statistical mechanics-based framework that provides a variable strength distribution depending on the structure's size and load configuration (Section 2.1). The framework utilizes five independent model parameters, which remain constant while capturing these variations (Section 2.2). In this study, the parameters are identified using maximum likelihood estimations (Section 2.3). Section 2.4 details bending strength data from both experimental and numerical studies. Since the experimental data available in the literature is insufficient to identify all five parameters, numerical simulations were primarily used. To validate the findings, a comprehensive dataset consisting of 556 homogeneous GLT beams from nine experimental studies [1–10] conducted over the past 38 years is presented.

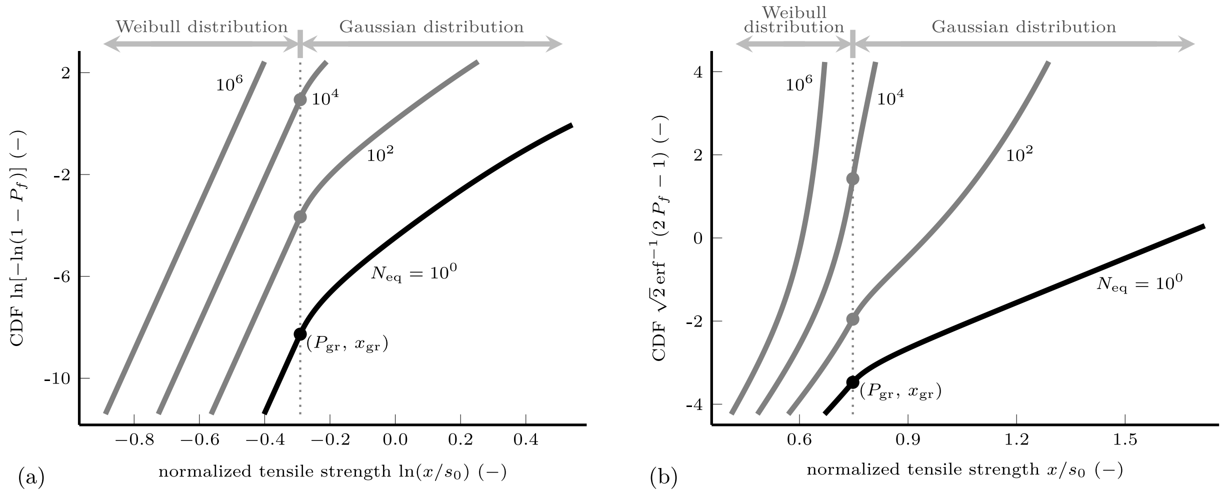

Fig. 1. CDFs of the tensile strengths for single and multiple equivalent elements N_{eq} shown in (a) Weibull probability plot and (b) normal probability plot, where the corresponding distributions appear as straight lines.

2.1. Finite weakest-link theory

The finite weakest-link theory provides PDFs for quasi-brittle materials of various sizes under different loading conditions. Bažant [20] proposed a gradual transition of the PDF from a predominantly Gaussian distribution (ductile failure) to a Weibull distribution (brittle failure) with increasing structural size. The theory is based on representative volume elements (RVEs),[1] whose failure causes the failure of the entire structure [21].

First, the representation of a single RVE under pure tensile loading is addressed, before expanding to structures of various sizes and their stress distributions based on loading conditions. For quasi-brittle materials, a single RVE must be capable of manifesting damage on smaller scales, such as microcracking, without leading to complete failure. Bažant and Le [30] argue that the ultimate strength of ductile materials follows a Gaussian distribution, based on the central limit theorem, as it sums all contributions across the failure surface. In contrast, Weibull's statistical strength theory [17] applies to brittle materials. Therefore, the type of PDF for a single RVE is a key consideration, as it cannot be purely Gaussian (ductile materials) nor purely Weibull (brittle materials).

In Le et al. [29], the PDF type of a single RVE is derived based on two statistical models: series coupling (chain model or weakest-link model) and parallel coupling (fiber bundle model). The gap between failure within the atomic lattice (nano-scale) and the RVE (macro-scale) was bridged using a hierarchical statistical model with sub-chains and sub-bundles. At the lowest scale (nano-scale), the PDF exhibited a power-law tail, and the mechanical post-peak behavior of elements in the fiber bundles was either brittle, linear softening, or plastic. Despite these different mechanical behaviors, the PDF type was consistent and could be formulated by a Gaussian distribution with a grafted far-left Weibull tail.

The cumulative distribution function (CDF) of the tensile strength of a single RVE P_1 (Fig. 1) follows a Weibull-Gaussian distribution [29]

$$P_1(x) = \begin{cases} 1 - \exp\left[-\left(\frac{x}{s_0}\right)^m\right] & \text{for} \quad x < x_{\mathrm{gr}} \\ P_{\mathrm{gr}} + \frac{r_{\mathrm{f}}}{\delta_{\mathrm{G}}\sqrt{2\pi}} \int_{x_{\mathrm{gr}}}^{x} \exp\left[-\frac{(x'-\mu_{\mathrm{G}})^2}{2\,\delta_{\mathrm{G}}^2}\right] \mathrm{d}x' & \text{for} \quad x \geq x_{\mathrm{gr}} \end{cases}, \tag{1}$$

where m is the Weibull modulus and s_0 is the scaling parameter of the Gaussian distribution. μ_{G} is the mean and δ_{G} is the standard deviation of the Gaussian distribution. P_{gr} is the probability at the grafting point x_{gr}, and r_{f} is a scaling parameter to normalize the grafted CDF to guarantee that $P_1(\infty) = 1$. To ensure the grafted CDF is a differentiable function [22], continuity of the probability density function must be guaranteed at the grafting point $p_1(x_{\mathrm{gr}}) = \left.\frac{\mathrm{d}P_1(x)}{\mathrm{d}x}\right|_{x=x_{\mathrm{gr}}}$, i.e.,

$$p_1(x_{\mathrm{gr}}^-) = p_1(x_{\mathrm{gr}}^+)\,. \tag{2}$$

Finally, the CDF of strength for an entire structure P_f is derived by constructing a conceptual chain of RVEs (Fig. 1), employing extreme value statistics

$$P_f(x) = 1 - (1 - P_1(x))^{N_{\mathrm{eq}}}\,, \tag{3}$$

where N_{eq} represents the equivalent number of RVEs within the chain. N_{eq} depends on the structure's size, loading condition, and RVE size,

$$N_{\mathrm{eq}} = \frac{V}{V_{\mathrm{RVE}}} \int_V \left[\langle\bar{\sigma}(\xi)\rangle\right]^m \mathrm{d}\xi\,, \tag{4}$$

where V is the structure's volume, V_{RVE} is the volume of a single RVE, $\bar{\sigma}$ represents the dimensionless stress distribution with parameterized spatial coordinates ξ, and m is the Weibull modulus. The Macaulay brackets $\langle\cdot\rangle$ are applied with the general formulation to consider only tensile stresses, which are responsible for (quasi-)brittle failure

$$\langle x\rangle = \begin{cases} x < 0: & 0 \\ x \geq 0: & x \end{cases}. \tag{5}$$

The finite weakest-link theory is a statistical model that uses the elastic stress field to qualitatively capture the nonlinear failure behavior of quasi-brittle materials [31]. Some of the presented parameters are interrelated, such as μ_{G} and δ_{G} depending, for example, on m, s_0, and x_{gr}. The introduction of independent parameters is addressed next.

2.2. Defining the model parameters

The model presented by Bažant and Pang [21,22] depends on five parameters: the Weibull modulus m, the scale parameter s_0, the probability at the grafting point P_{gr}, the CV of the Weibull-Gaussian distribution ω_0, and the volume of a single RVE V_{RVE}. The last parameter controls the size- and load-dependent scaling of the grafted Weibull-Gaussian CDF according to Eqs. (3) and (4). The other four parameters are presented next and deal with the PDF of a single RVE.

Starting with the Weibull part of the distribution in Eq. (1), the Weibull modulus m controls the slope and the scale parameter s_0 the horizontal position of the distribution on the Weibull probability plot (Fig. 2a). The Gaussian part of the distribution in Eq. (1) depends on its mean and standard deviation, μ_{G} and δ_{G}, respectively. These two parameters are related to the Weibull-part parameters to fulfill the continuity condition in Eq. (2) at the grafting point. This limits their

[1] The RVE size differs in comparison to elastic homogenization theory [21].

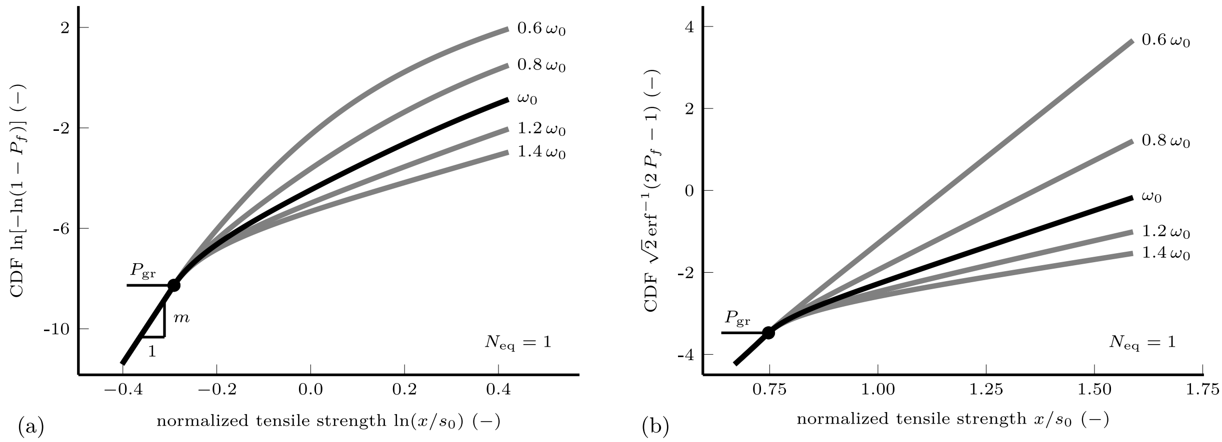

Fig. 2. Parameters (m, s_0, P_{gr}, ω_0) that define the CDF of the tensile strength for a single equivalent element N_{eq} shown in (a) Weibull probability plot and (b) normal probability plot.

effectiveness, as the goal is to have independent parameters. Thus, the grafting point probability P_{gr} and the CV of a single RVE ω_0 are used instead from now on.

P_{gr} defines the position of the grafting point x_{gr}, where the Weibull distribution transitions to the Gaussian one (Fig. 2). The grafting point position reads

$$x_{gr} = s_0\left[-\ln\left(1-P_{gr}\right)\right]^{1/m}, \tag{6}$$

based on the Weibull part of the Weibull-Gaussian distribution in Eq. (1). At x_{gr}, the continuity condition from Eq. (2) is used to formulate the Gaussian mean

$$\mu_G = x_{gr} + \delta_G\left[-2\ln(g)\right]^{1/2} \tag{7}$$

with

$$g = \frac{\sqrt{2\pi}\, m\, \delta_G}{s_0}\left(\frac{x_{gr}}{s_0}\right)^{m-1}\exp\left(-\left(\frac{x_{gr}}{s_0}\right)^{m}\right). \tag{8}$$

μ_G is now a function of δ_G, and for its computation, it is necessary to restrict g to the range $0 < g \le 1$.

The last step is to find an expression for δ_G, which is provided by the CV

$$\omega_0 = \frac{\delta_0}{\mu_0}, \tag{9}$$

where the mean reads as:

$$\mu_0 = \int_0^{\infty} x\, p_1(x)\,\mathrm{d}x \tag{10}$$

and standard deviation as:

$$\delta_0 = \left[\int_0^{\infty}\left(x-\mu_0\right)^2 p_1(x)\,\mathrm{d}x\right]^{1/2}, \tag{11}$$

both regarding the Weibull-Gaussian distribution of a single RVE. Plugging Eq. (7) in Eq. (1) and differentiate with respect to x leads to the probability density function of a single RVE p_1, which is then used in Eqs. (10) and (11). This finally leaves δ_G as the only variable in the formulation of ω_0 in Eq. (9). δ_G is found numerically for a given ω_0 by

$$\underset{\delta_G}{\arg\min}\begin{cases} 0<g<1: & \left|\omega_0-\frac{\delta_0}{\mu_0}\right| \\ g\le 0: & \lambda\,(g-1)^2 \\ g\ge 1: & \lambda\, g^2 \end{cases}, \tag{12}$$

where λ is a Lagrangian multiplier and g is defined by Eq. (8).

2.3. Parameter fitting

The aim is for the grafted Weibull-Gaussian distribution to accurately describe the observed data. To achieve this, the discussed parameters (m, s_0, P_{gr}, ω_0, and V_{RVE}) are fitted to either experimentally or numerically obtained data. The maximum likelihood method is commonly used to estimate the parameters $\boldsymbol{\theta}$ of the probability density function p_f for a set of observed data $\boldsymbol{x}$, which is obtained by differentiating Eq. (3) with respect to x. The estimates are obtained by maximizing the likelihood function

$$\mathcal{L}(\boldsymbol{\theta}|\boldsymbol{x}) = \prod_{i=1}^{n} p_f(x_i;\boldsymbol{\theta}). \tag{13}$$

To estimate the five discussed parameters $\boldsymbol{\theta} = [m, s_0, P_{gr}, \omega_0, V_{RVE}]$, the natural logarithm of $\mathcal{L}(\boldsymbol{\theta}|\boldsymbol{x})$ is maximized for k given sets of observed data $\boldsymbol{x}_k$. This leads to the minimization problem that is solved numerically by

$$\underset{\boldsymbol{\theta}}{\arg\min}\; -\sum_{j=1}^{k}\ln\left(\mathcal{L}(\boldsymbol{\theta}|\boldsymbol{x}_j)\right) + \lambda\, h, \tag{14}$$

where λ is a Lagrangian multiplier and

$$h = \langle -P_{gr}\rangle^2 \tag{15}$$

is a penalty function to ensure that $P_{gr} > 0$. To maintain the integrity of the model during the optimization, P_{gr} is set to zero for values violating the constraint $P_{gr} > 0$.

2.4. Experiments and simulations

Estimating the parameters for GLT beams requires data on their tensile or bending strength. This data must encompass both the Weibull and Gaussian parts of the distribution (Fig. 1) and can be obtained from experiments (Table 1) or simulations (Table 2). A significant challenge with experimentally obtained data is that the tested beam and sample sizes currently available in the literature are too small to provide sufficient information on the Weibull part (Fig. 3a). Simulations can effectively fill this gap, providing the necessary information for now (Fig. 3b). In this study, the empirical CDF for both experimental and simulated data was always determined using the method proposed by Hazen [33]: $P_f = (i-0.5)/n$.

The challenge exists despite numerous studies in the literature [1–10] reporting the bending strength of homogeneous GLT beams manufactured from Norway spruce[2] (Table 1). Primarily, four-point bending tests (Fig. 4a) were used, in accordance to EN 408 [32]. The standard test setup prescribes the length-to-depth (ℓ/d) ratios between the bearing and loading points, leading to a proportional stress field for beams

[2] The studies [1,2,4] present properties aligning with Norway spruce without explicitly specifying the wood species.

Table 1
Experimental data from the literature on GLT beams with homogeneous layup considered in this study. Dimensions are in reference to Fig. 4.

Study	Sample size n	Dimensions in mm ℓ	ℓ_1	ℓ_2	w	d	Strength class Study[a]	Assigned[b]	Eq. no. RVEs[e] N_{eq}
Ehlbeck and Colling [1]	3	3750	1875	–	100	330	GK II[c]	GL24h	0.7
	3	3750	1375	1000	100	330	GK II[c]	GL24h	6.3
	3	4650	1325	2000	100	330	GK II[c]	GL24h	20.9
	3	6900	1700	3500	100	330	GK II[c]	GL24h	20.9
	3	6900	1700	3500	100	330	GK II[c]	GL24h	6.0
	6	3700	850	2000	100	167	GK II[b]	GL24h	9.0
	3	3300	650	2000	100	250	GK II[c]	GL24h	12.1
	3	4650	1325	2000	100	500	GK II[c]	GL24h	18.3
	3	6000	2000	2000	100	750	GK II[c]	GL24h	28.1
	3	9000	3500	2000	100	850	GK II[b]	GL24h	33.3
	3	7500	2750	2000	100	1000	GK II[c]	GL24h	38.3
	3	7500	2750	2000	100	1000	GK II[c]	GL24h	38.3
	3	11 800	4900	2000	100	1250	GK II[b]	GL24h	51.1
Colling [2]	7	7500	2750	2000	100	600	–[d]	22.8 $\mathrm{N/mm^2}$	23.0
	7	7500	2750	2000	100	600	–[d]	24.6 $\mathrm{N/mm^2}$	23.0
	7	7500	2750	2000	100	600	–[d]	24.9 $\mathrm{N/mm^2}$	23.0
	7	7500	2750	2000	100	600	–[d]	29.6 $\mathrm{N/mm^2}$	23.0
	7	7500	2750	2000	100	600	–[d]	32.6 $\mathrm{N/mm^2}$	23.0
	7	7500	2750	2000	100	600	–[d]	33.0 $\mathrm{N/mm^2}$	23.0
Falk et al. [3]	104	5400	1800	1800	90	300*	LH35	29.8 $\mathrm{N/mm^2}$	9.1
	112	5400	1800	1800	90	300*	LH40	34.1 $\mathrm{N/mm^2}$	9.1
Aasheim and Solli [4]	24	5400	1800	1800	90	300*	T30	GL28h	9.1
	20	10 800	3600	3600	90	600*	T30	GL28h	36.4
Gehri et al. [5]	23	5310	1770	1770	160	297*	MS10h	GL20h	15.7
(Schickhofer [6])	10	9504	2970	3564	160	594*	MS10h	GL20h	62.7
	30	5310	1770	1770	160	297*	MS13h	GL26h	15.7
	20	5310	1770	1770	160	297*	MS17h	GL30h	15.7
	18	9504	2970	3564	160	594*	MS17h	GL30h	62.7
Brandner et al. [7]	25	9000	2700	3600	160	600*	GL36h		63.6
Fink et al. [8]	12	5680	1880	1920	115	320*	GL24h		13.2
	12	5680	1880	1920	115	320*	GL36h		13.2
Kandler et al. [9]	10	2340	780	780	90	132*	GL24h		1.7
	10	5200	1610	1980	90	330*	GL24h		10.9
	10	2340	780	780	90	132*	GL30h		1.7
	10	4140	1380	1380	90	231*	GL30h		5.4
	10	5200	1610	1980	90	330*	GL30h		10.9
Fink et al. [10]	4	10 800	3600	3600	158	600*	GL24h		63.8
	2	18 000	6000	6000	178	1000*	GL24h		200
	4	10 800	3600	3600	158	600*	GL32h		63.8
	2	18 000	6000	6000	178	1000*	GL32h		200

* ℓ_i/d ratios according to EN 408 [32].
[a] As specified by each study.
[b] Assigned as specified in Appendix A.
[c] One beam's outermost lamination had grade GK I.
[d] Three outermost laminations graded according to specific wood properties.
[e] Equivalent number of RVEs from Eq. (4) for model parameters listed in Set 3 in Table 3.

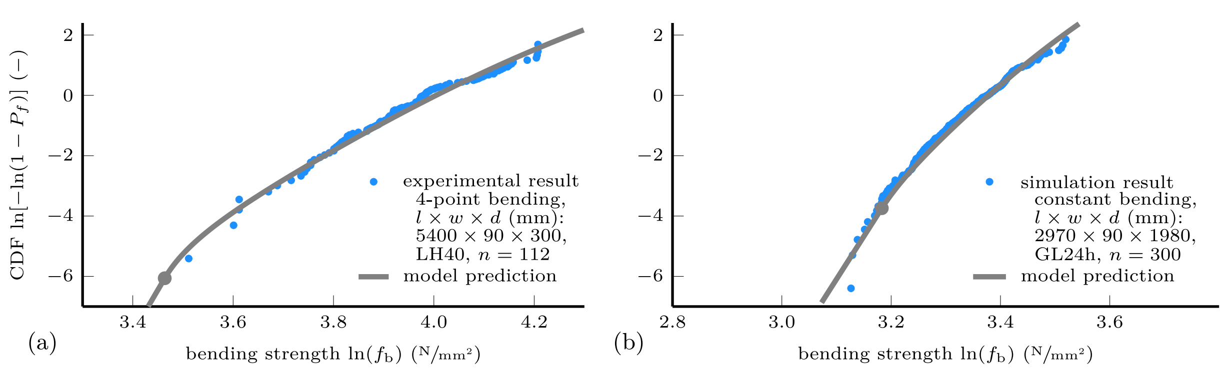

Fig. 3. Exemplary CDFs of the bending strength f_b in Weibull probability plots for (a) experimental results from [3] and (b) simulation results from [15], with model predictions using parameters from Set 2 and Set 1 in Table 3, respectively. The large dot marks the transition from the Weibull to the Gaussian distribution.

of varying sizes. A significant advantage of the finite weakest-link theory is its capability to consider such stress fields. Thus, studies with varying ℓ/d ratios or using a three-point bending test setup (Fig. 4b) can also be included.

A recent simulation campaign [15] investigated the size effect of large GLT beams. The simulations considered discrete vertical and horizontal cracks using the extended finite element method and cohesive surfaces, respectively, as provided by the frameworks available

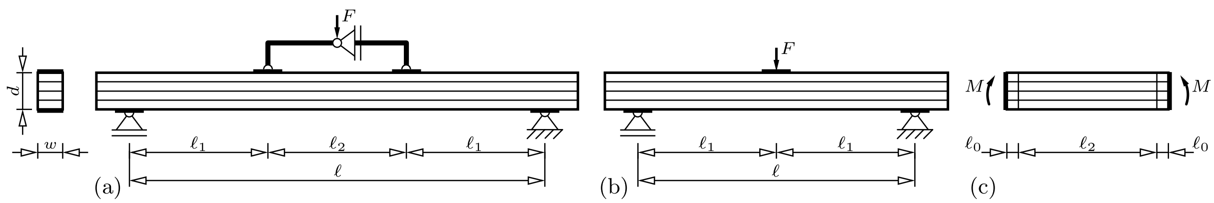

Fig. 4. Load configurations for GLT beams: (a) four-point bending test, (b) three-point bending test, and (c) directly applied constant bending moment. The span of the beam is denoted by ℓ, with ℓ_1 and ℓ_2 representing the ranges with triangular and constant bending moment profiles, respectively. ℓ_0 was implemented in the simulations to minimize load application effects, where no damage was considered. w is the beam width and d the depth.

Table 2
Simulated data from [15] on GLT beams with homogeneous layup, as considered in this study. Dimensions are in reference to Fig. 4c.

		Dimensions in mm[b]		
ℓ/d	Sample size[a] n	ℓ_2	d	Eq. no. RVEs[c] N_{eq}
1.5	1600	247.5	165	0.6
	400	495	330	2.6
	400	990	660	10.3
	400	1980	1320	41.2
	300	2970	1980	92.7
	200	3960	2640	165
	200	4950	3300	257
6.0	500	990	165*	2.6
	100	1980	330*	10.3
	100	3960	660*	41.2

* ℓ_2/d ratio according to EN 408 [32].
[a] For each strength class: GL24h and GL30h.
[b] Constant width $w = 90\,\text{mm}$.
[c] Equivalent number of RVEs from Eq. (4) for model parameters listed in Set 1 in Table 3.

Table 3
Model parameters for a single RVE: m (Weibull modulus), s_0 (scale parameter), P_{gr} (failure probability at grafting point), ω_0 (CV of a single RVE), and V_{RVE} (RVE volume). $f_{b,ref}$ is the characteristic reference bending strength.

		Weibull-Gaussian parameters				
Parameter sets	Strength class	m (−)	s_0 (N/mm²)	P_{gr} ($\times 10^{-4}$)	ω_0 (−)	V_{RVE} (mm³)
Set 1[a]	GL24h GL30h	28.4	32.27 37.93	2.562	0.1218	97087
Set 2	LH35 LH40	28.4	**35.74**[c] **42.73**[c]	2.562	**0.1717**[b]	97087
Set 3	$f_{b,ref}$	28.4	**1.260 $f_{b,ref}$**[d]	2.562	0.1717	97087

[a] Fitted to simulation results [15].
[b] Tuned by experimental results [3].
[c] Adjusted to strength classes from [3].
[d] Related to European strength classes [12].

Table 4
Maximum absolute values of relative errors between empirical simulation results and model predictions for 20 configurations (16 configurations in parentheses).

		Maximum absolute values of relative errors[a] (%)					
ℓ/d	Strength class	5th percentile		mean		95th percentile	
1.5	GL24h	9.0	(3.3)	2.7	(1.1)	4.1	(4.1)
	GL30h	4.3	(2.3)	6.0	(2.2)	8.5	(4.1)
6.0	GL24h	8.2	(1.4)	4.1	(3.3)	0.6	(0.6)
	GL30h	3.8	(3.8)	2.1	(1.6)	3.4	(0.6)
Summary		9.0	(3.8)	6.0	(3.3)	8.5	(4.1)

[a] Parentheses (·) denote results that exclude simulations of the smallest size.

in Abaqus [34]. Beams with depths up to 660 mm accounted for plastic deformations with a multisurface failure criterion [35–37] in the upper half of the beam. In this study, we used data from 8400 simulated GLT beam sections (Table 2), encompassing two strength classes, GL24h and GL30h, for ℓ/d ratios of 1.5 and 6.0. The beam depths ranged from 165 mm to 3300 mm, and the sections were subjected to a constant bending moment (Fig. 4c).

In the finite weakest-link framework, the stress distribution and beam size is accounted for by the equivalent number of RVEs N_{eq}, calculated according to Eq. (4) in conjunction with the model parameters identified in Section 3 (Table 3). N_{eq} values are provided for experimental data in Table 1 and for simulation data in Table 2.

3. Model based on the finite weakest-link theory framework

Based on the estimated model parameters (Section 3.1), the model predictions are compared to experimental results from the literature (Section 3.2). This section concludes with discussions of the model parameters (Section 3.3).

3.1. Estimating the model parameters

The five model parameters (m, s_0, P_{gr}, ω_0, and V_{RVE}) for the Weibull-Gaussian distribution were initially estimated using results from numerical simulations [15]. Subsequently, ω_0 was refined based on data from a comprehensive experimental study [3] and s_0 was linked to European strength classes [12]. These steps resulted in individual parameter sets presented in Table 3, with the final parameters given in Set 3.

The initial parameter estimation was based on numerical simulations with $\ell/d = 1.5$ from Table 2, using the likelihood function maximization according to Eq. (14). Parameters were estimated from data of both strength classes, except for the scale parameter s_0, which was estimated separately for each strength class (Set 1 in Table 3). The model's versatility was demonstrated by formulating the PDFs for all 20 simulated beam configurations using only the six fitted parameters (Fig. 5). The size differences were accounted for by employing the equivalent number of RVEs N_{eq} (Table 2). The maximum absolute values of the relative errors of the 5th percentile, mean, and 95th percentile of the grafted Weibull-Gaussian distribution, compared to the simulation data, showed the model's adequacy (Table 4). The largest deviations were observed for the smallest simulated beam sections.

The experimental results presented by Falk et al. [3] were well-suited for additional analysis due to the extensive scope of their experiments. To derive the corresponding Weibull-Gaussian distribution, the previously estimated parameters (Set 1 in Table 3) were used, except for the scale parameter s_0, which was adjusted for each strength class. The equivalent number of RVEs N_{eq} accounted for the beam size and load configuration (Table 2). A comparison between the empirical CDFs and the CDFs of the initial model prediction revealed a significant difference in the standard deviation for both strength classes (Fig. 6a). This discrepancy was attributed to the limited sample size of 140 wooden boards per strength class available for the simulation campaign. As a result, the CV ω_0 was tuned, along with the corresponding scale parameters s_0, based on the experimental data (Set 2 in Table 3), ensuring better alignment with the empirical CDF (Fig. 6a).

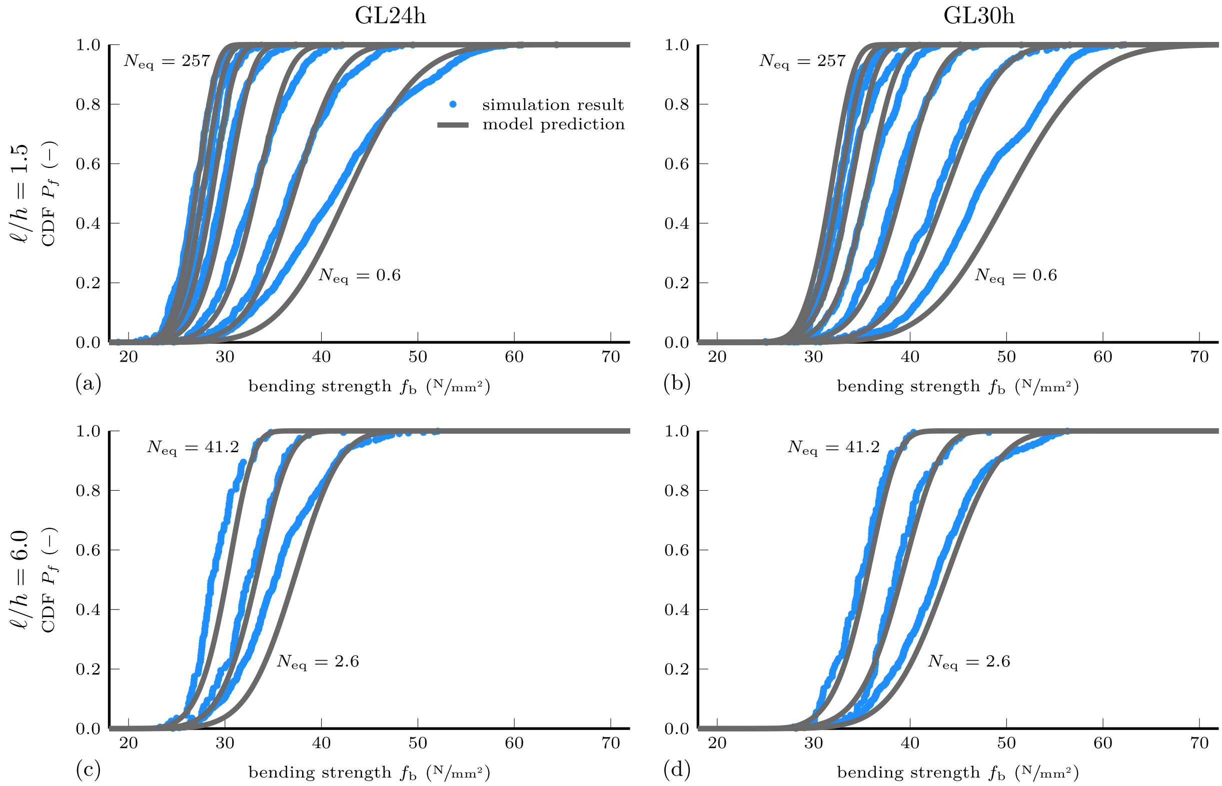

Fig. 5. CDFs of the simulated and model predicted bending strengths f_b for beam sections subjected to a constant bending moment, as outlined in Table 2. Model predictions use parameters from Set 1 in Table 3, considering different sizes through the equivalent number of RVEs N_{eq}. The length-to-depth ratios ℓ/d are (a,b) 1.5 and (c,d) 6.0 with strength classes (a,c) GL24h and (b,d) GL30h.

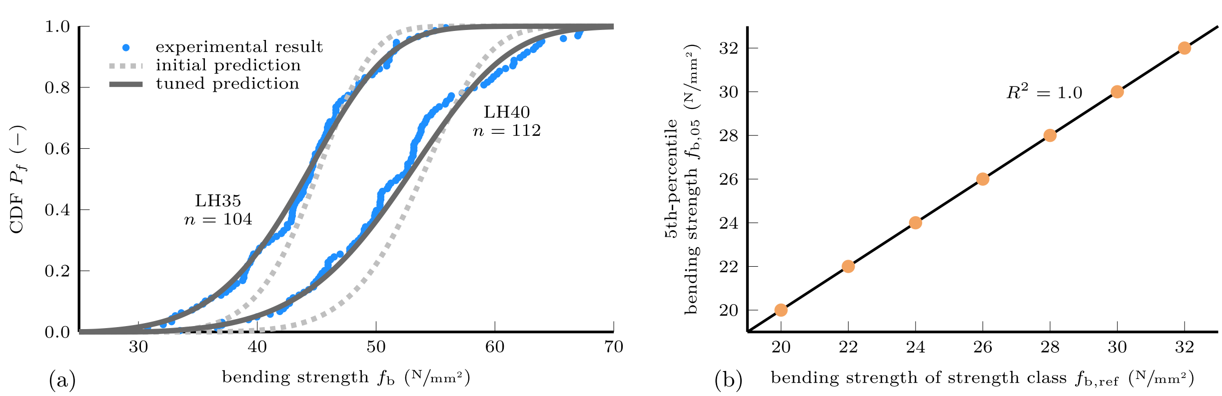

Fig. 6. Adjusting the model parameters involves two steps: (a) tuning the CV ω_0 based on experimental results from [3], resulting in the parameters from Set 2 in Table 3 for the tuned model prediction; and (b) relating the scale parameter s_0 to strength classes by matching their 5th-percentile bending strengths $f_{b,ref} = f_{b,05}$ for the reference beam size and test setup, as defined in Eqs. (17) and (18), respectively.

Additionally, the scale parameter s_0 was linked to strength classes by using a reference bending strength $f_{b,ref}$. This relation was established by

$$s_0 = \hat{s}_0 \, f_{b,ref} \,, \tag{16}$$

where $\hat{s}_0$ denotes the scaling factor, and $f_{b,ref}$ corresponds to the characteristic (5th-percentile) bending strength associated with a specific reference beam size and test configuration. The reference beam had the length ℓ, width w, and depth d of:

$$\ell = 10\,800\,\mathrm{mm}, \quad w = 150\,\mathrm{mm}, \quad d = 600\,\mathrm{mm}\,. \tag{17}$$

The reference test configuration was a four-point bending test with the beam span depending on d and loading applied at the third-points:

$$\ell = 18\,d, \quad \ell_1 = 6\,d, \quad \ell_1 = \ell_2\,. \tag{18}$$

The load configuration with the corresponding dimensions is illustrated in Fig. 4a. These specifications were chosen to align the Weibull-Gaussian distributions with the strength classes defined in EN 14080 [12].

The scaling factor $\hat{s}_0$ was then determined through numerical optimization to ensure that the 5th percentile of the Weibull-Gaussian distribution matched the given $f_{b,ref}$ (Fig. 6b; Set 3 in Table 3). The optimization used the previously established parameters (Set 2 in Table 3), along with the definitions of the reference beam size and test configuration from Eqs. (17) and (18), respectively. This resulted in an $N_{eq} = 61$ used for the model predictions.

In conclusion, the parameters m, P_{gr}, and V_{RVE} were determined through simulations. The CV ω_0 was tuned based on the experimental study by Falk et al. [3]. Finally, the scale parameter s_0 was related to the characteristic reference bending strength using Eq. (16), enabling the use of European strength classes [12]. The parameters are summarized under Set 3 in Table 3.

3.2. Analysis of model prediction and experimental results

The statistical mechanics-based model generates PDFs for GLT beams of various strength classes, sizes, and load configurations. This enabled a comparison with results from the nine experimental studies listed in Table 1, encompassing data from 40 test series that include 556 beams with a homogeneous layup published over the past 38 years. The sample sizes varied significantly across the test series, with some containing as few as two or three tests. The beam sizes ranged from depths of 132 mm to 1000 mm for beams subjected to a test setups following EN 408 [32].

Analyzing such a large experimental dataset, some scatter in the data was expected, as many influencing factors differ from study to study. Fink et al. [16] listed examples of such influences, including wood species, material source, finger-joint quality, beam dimensions, and test setup. They also pointed out that variations can be caused by different batches of wooden boards, different producers, and specific characteristics of the strength class. Despite these variations, an observable trend was anticipated. To facilitate the comparison of the different strength classes used in the studies, the strength was normalized by the scale parameter s_0.

The analysis compared the mean bending strength $\bar{f}_\mathrm{b}$ and the coefficient of variation (CV) of the bending strength ω_f between the model predictions and the experimental results. The CV

$$\omega_f = \frac{\delta_f}{\bar{f}_\mathrm{b}} \tag{19}$$

is the ratio of the standard deviation δf of the bending strength to $\bar{f}_\mathrm{b}$. The calculation of δf and $\bar{f}_\mathrm{b}$ for both the experimental results and model predictions is detailed in Appendix B. The varying beam sizes and load configurations were accounted for using Neq from Eq. (4), which depends on the model parameters m and V_RVE. The analysis used the five optimal parameters from Set 3, with the corresponding N_eq values for the experimental sets shown in Table 1.

The predicted bending strength agreed well with the experimental results (Fig. 7). More than three-fourths of the experimental results lay within a range ± 10% of the model prediction (Fig. 7a). The predicted decrease followed the experimental observations of mean bending strength for an increasing N_eq. The relative error of all 40 sets, relative to their prediction, showed that the mean aligns very well with the model prediction, having a standard deviation $\delta = 0.0862$ (Fig. 7b). A linear regression with an intercept close to zero and a slope of 1.03 confirmed the correct inclusion of different strength classes, beam sizes, and test setup configurations of the model (Fig. 7c). The coefficient of determination was $R^2 = 0.818$.

The predicted CV also agreed well with the experimental results considering the rather small sample size of some sets (Fig. 8). Although the large tested beams had a very small sample size, the CV showed a decreasing trend for an increasing N_eq (Fig. 8a). Considering the sets with 10 or more tests relative to their prediction, the mean of the relative errors aligned very well with the model prediction, having a standard deviation $\delta = 0.141$ (Fig. 8b). The linear regression highlighted the challenge of comparing a universal model with individual experimental sets (Fig. 8c). For example, the current model predicts a constant ω_f for a given beam size and test setup, but it cannot capture the variability observed by Colling [2].

3.3. Discussion of the model parameters

In the following, the focus is on discussing the expected order and range of the five model parameters and comparing them to the optimal parameters from Set 3 in Table 3.

Weibull modulus

Determining the Weibull modulus m experimentally is challenging. While the Weibull distribution features a constant CV inversely proportional to m, calculating m directly from the CV is not straightforward. The Weibull part of the Weibull-Gaussian distribution becomes dominant only in sufficiently large structures. Bažant and Novák [38] demonstrated that testing concrete beams of the required size would be practically infeasible, and this limitation also applies to GLT beams.

Data of typically tested beam sizes in the literature lack information on the Weibull part in the Weibull-Gaussian distribution, suggesting that the Weibull part only represents very low probabilities. Observing this range experimentally would require large enough sample sizes. For instance, Falk et al. [3] tested homogeneous GLT beams with a depth $d = 0.3$ m, including two strength classes with over 100 specimens each. Their lowest results correspond to empirical values $P_f < 1\%$. Despite this extensive testing, the data from both strength classes failed to reveal the transition from a Weibull to a Gaussian distribution (Fig. 3a). This highlights the practical infeasibility of such experiments, given the necessity for even larger sample sizes.

Another method to calculate m involves using experimental results from two different beam sizes with proportional stress distributions, denoted with subscripts $i = 1, 2$. Based on Weibull's statistical strength theory [17], m can be determined by

$$\frac{f_2}{f_1} = \left(\frac{V_1}{V_2}\right)^{1/m}, \tag{20}$$

where f_i denotes the strength and V_i the tensile stressed volume of the beam. To determine the desired m that describes the asymptotic limit for the strength decrease, the strengths f_i need to be obtained from the Weibull part. A smaller strength decrease corresponds to a larger m, whereas a larger decrease corresponds to a smaller m, assuming the same volume ratio.

Aasheim and Solli [4] and Schickhofer [6] tested different beam sizes, resulting in m values around 20 and 35, respectively. These values were obtained using Eq. (20) with f_i corresponding to their reported 5th-percentile values.[3] Notably, the smaller beam size in both studies was $d \approx 0.3$ m, which is too small to capture the 5th percentile from the Weibull distribution part, as previously described. Therefore, these m values represent a lower limit, as the strength decrease gets smaller for larger structures, approaching the trend solely defined by the desired (theoretically higher) m. The value identified through simulations, $m \approx 28$, appears reasonable in this context.

Given wood's orthotropic nature, a further question arises: Does m vary with the material direction, given that Weibull's statistical strength theory [17] is designed for isotropic materials? If m is independent of material direction, changing volume in any direction will not affect the CV, which depends solely on m and must remain constant [18]. This implies defects should be evenly distributed across all material directions. However, this uniform defect distribution does not hold true in timber. For example, knots appear quite regularly in the longitudinal direction of boards, but their position across the board's width can vary significantly, likely leading to different effects on the width of GLT beams. Design codes implement different strategies for considering beam width. For instance, prEN 1995-1-1 [11] excludes the width, while ANSI/AWC NDS [39] considers all three spatial dimensions with the same m. For the present model, we included the width and applied the same m, which can be easily adapted as new data becomes available.

Scale parameter

The scale parameter s_0 adjusts the strength range covered by the Weibull-Gaussian distribution while maintaining a constant CV. In

[3] The 5th percentiles were obtained from a three-parameter Weibull distribution in [4] and a Gaussian distribution in [6].

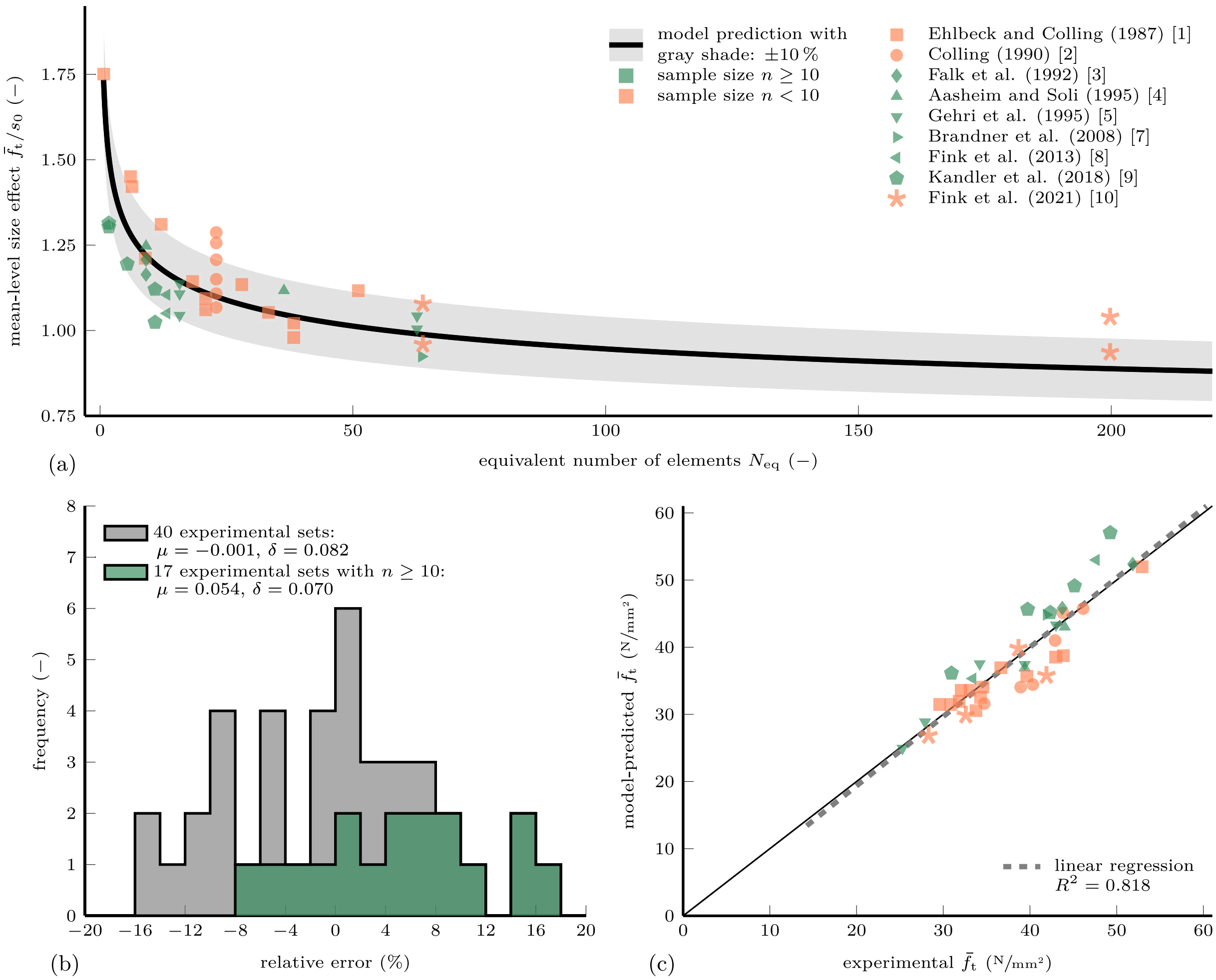

Fig. 7. Analysis of model prediction and experimental results for the mean bending strength $\bar{f}_b$ showing (a) the effect on $\bar{f}_b$ normalized by s_0 depending on the equivalent number of elements N_{eq}, (b) histogram of relative errors, and (c) linear regression.

Section 3.1, s_0 was related to the 5th-percentile bending strength for the reference beam size and test setup, as defined by Eqs. (17) and (18). This relation ensures the model accurately represents the European strength classes [12].

Grafting point probability

According to Bažant and Pang [22], the grafting point probability P_{gr} for a single RVE is assumed to be in the range of 0.0001 to 0.01 to ensure the transition between Gaussian and Weibull distributions is observable for typical sizes of tested structures. The identified $P_{gr} \approx 0.0003$ from simulations falls on the lower end of this range, indicating that the Weibull distribution part will only be observable for quite large structures. As discussed regarding the Weibull modulus, this appears to be the case for GLT beams.

CV of a single RVE

The CV of a single RVE ω_0 was tuned using data from an experimental study [3]. This parameter tuning allowed the model to closely match the mean values of the experimental data presented (Fig. 8). However, the scattering observed in the experiments, especially those with only a few samples, underscores the importance of sample size in test series.

RVE volume

For orthotropic materials, the volume of a single RVE (V_{RVE}) derives from dimensions (length, width, and depth) that vary based on material direction [29]. According to Le et al. [29], the RVE size is likely comparable to the length of the FPZ observed in size effect tests proposed by Bažant et al. [40]. Recently, Le et al. [31] found that V_{RVE} is a structural parameter related to Irwin's characteristic length and the crack band width, with their relationship varying according to the load configuration.

In the context of timber, the pronounced heterogeneity caused by defects such as knots poses a challenge when utilizing parameters from fracture mechanics. Timber is characterized by both the wood species and the grading process, which manages such defects. Consequently, the size of the RVE likely depends on the wood species, the grading process, and the specific load configuration.

With limited information on timber, materials like concrete or ceramics suggest a rule of thumb where the characteristic length is roughly two to three times the maximum inhomogeneity size [22]. Consequently, the anticipated dimensions of wooden RVEs range from millimeters to centimeters, which aligns well with the obtained $V_{RVE} \approx 100\,000\,\text{mm}^3$. This volume corresponds to a wooden cube with a side length of approximately 46 mm, which appears intuitively plausible.

4. Dependency on beam size and load configuration

Of great interest are the trends of $\bar{f}_b$ and ω_f for beams larger than those experimentally tested. For example, these two parameters already define a two-parameter PDF, which can be further utilized in a structural reliability analysis (Section 5). Both the model and the experimental data suggest further decreasing trends with increasing beam size, as can be seen from Figs. 7a and 8a. This section presents the

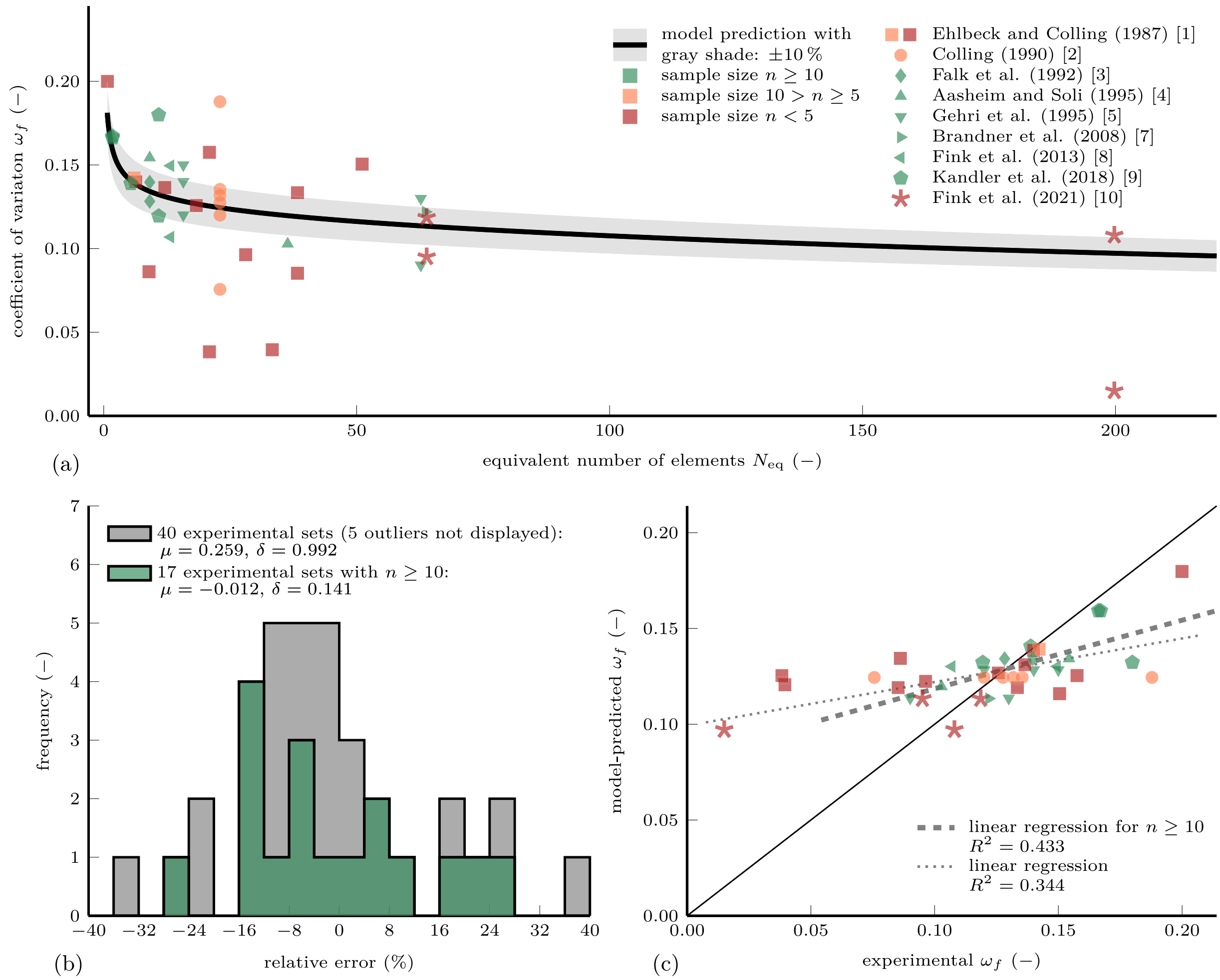

Fig. 8. Analysis of model prediction and experimental results for the CV ω_f showing (a) the effect on ω_f depending on the equivalent number of elements N_{eq}, (b) histogram of relative errors, and (c) linear regression.

model's predictions for trends extending beyond the tested beam sizes, using the optimal parameters from Section 3 (Set 3 from Table 3).

The trends of $\bar{f}_{\mathrm{b}}$ and ω_f continued to decrease for large beams, as shown by Fig. 9. The variation decreased significantly with decreasing mean bending strength. The experimental studies [5,7,10] included sets of beams with dimensions very close to the reference size having a depth $d = 0.6\,\mathrm{m}$ (Table 1). Calculating their mean CV resulted in $\omega_f = 0.111$ (values ranged from 0.090 to 0.130), which was within 2% of the model prediction. For the reference beam in the reference test setup, the relationship between the mean bending strength and the 5th percentile strength was $\bar{f}_{\mathrm{b}} = 1.25\, f_{\mathrm{b,ref}}$. This result is only slightly different from the relationship $\bar{f}_{\mathrm{b}} = 1.29\, f_{\mathrm{b,ref}}$, which is obtained by following JCSS [28] recommendations to use a log-normal distribution for f_{b} with $\omega_f = 0.15$.

Frese and Blaß [14] conducted a simulation study on homogeneous GLT beams of different strength classes and beam sizes. For the simulated reference-sized beams, ω_f ranged from 0.133 to 0.149, which was close to the JCSS [28] recommendation for f_{b} with $\omega_f = 0.15$. For beams with depths of up to 3 m, ω_f ranged from 0.080 to 0.087. In both cases, their values were larger than the predicted value presented herein (Fig. 9). On the other hand, the decrease in $\bar{f}_{\mathrm{b}}$ aligned well with the herein presented value of 0.774, which was close to the edge of the observed range of 0.755 to 0.779 in [14].

A big advantage of the presented model is the flexibility to account for different load configurations (stress fields) by the equivalent number of elements N_{eq}, as given in Eq. (4). Thus, one specific probability distribution can correspond to multiple scenarios, where beams have different sizes and load configurations. In Fig. 9, each marked beam corresponds to a specific probability distribution, where the size of the beam depends on the load configuration (examples given in Table 5). The examples highlight how dependent PDFs are on the stress distribution.

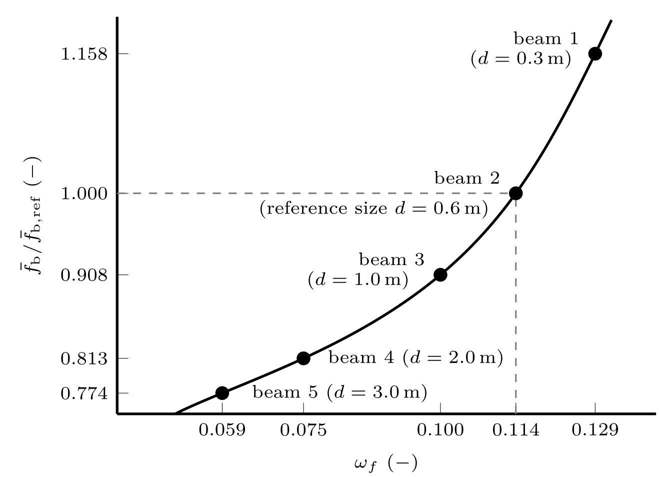

Fig. 9. Interaction of CV ω_f and mean bending strength $\bar{f}_{\mathrm{b}}$ normalized by the mean reference bending strength $\bar{f}_{\mathrm{b,ref}}$ highlighting exemplary beams with dimensions given in Table 5.

Table 5
Homogeneous GLT beams with the same cross-section dimensions and equivalent number of elements N_{eq} result in different beam lengths when subjected to three exemplary load configurations.

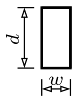

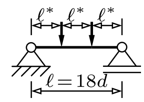

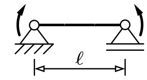

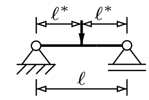

		Cross section		4-point bending[a]		constant bending	3-point bending	
Beam	Eq. no. RVEs[c] N_{eq} (−)	w (m)	d (m)	ℓ (m)	ℓ^* (m)	ℓ (m)	ℓ (m)	ℓ^* (m)
1	15		0.3	5.4	1.8	1.9	56.5	28.3
2[b]	61		0.6	10.8	3.6	3.8	113.1	56.5
3	168	0.15	1.0	18.0	6.0	6.4	188.4	94.2
4	673		2.0	36.0	12.0	12.8	376.9	188.4
5	1515		3.0	54.0	18.0	19.2	565.3	282.7

[a] Reference test setup according to Eq. (18).
[b] The dimensions in 4-point bending equal the reference beam size according to Eq. (17).
[c] Equivalent number of RVEs from Eq. (4) for model parameters listed in Set 3 in Table 3.

The experimental data presented included various load configurations, primarily four-point bending tests, with only some following EN 408 [32]. One set of beams applied three-point bending tests (Table 1, first set in [1]), with results aligning well with the model prediction (Figs. 7 and 8, lowest N_{eq} in [1]). Furthermore, the model was able to predict pure tensile strengths. The characteristic tensile strength $f_{t,05}$ of GLT beams modeled according to EN 408 [32] showed a ratio $f_{t,05}/f_{b,05} = 0.84$ compared to the 0.8 used in EN 14080 [12]. Frese et al. [41] found a ratio of 0.88 based on a numerical study. Nevertheless, studies exploring different load configurations experimentally are rather limited in the literature.

5. Exemplary structural reliability analysis

The effect of decreasing mean bending strength $\bar{f}_b$ and CV ω_f with increasing beam size on the probability of failure P_f is critical for a holistic design, aiming to maintain a constant level of safety regardless of structure size. Considering only the decrease in strength without accounting for the also decreasing CV might result in inefficient designs. The section first outlines the procedure for the conducted structural reliability analysis (Section 5.1). To investigate the effects of decreasing trends, a simple design example with a single load effect and resistance modeled by either a grafted Weibull-Gaussian or log-normal distribution is presented (Section 5.2). The discussion covers the results based on the two different resistance distributions (Section 5.3) and the sensitivity with a decreased Weibull modulus m for the Weibull-Gaussian distribution (Section 5.4).

The analysis excludes uncertainties in the modeled load effect and resistance, as well as load duration effects and moisture influences. Fink et al. [16] discuss various sources of variation that need to be considered in such an analysis, which were already mentioned in Section 2.4. In this context, it is notable that the model does not provide the 5th percentile with a 75% tolerance limit as required by EN 14358 [27].

5.1. Procedure and definitions

To analyze the structural reliability, PDFs are assigned to the load effect S and the resistance R. For independent S and R, the structure's probability of failure P_f can be determined using the convolution integral

$$P_f = \int_0^\infty P_R(x)\, p_S(x)\, dx\,, \tag{21}$$

where P_R is the CDF of the resistance and p_S is the probability density function of the load effect [42]. The integral was solved numerically using adaptive Gauss–Kronrod quadrature. The relationship between P_f and the reliability index β is expressed by

$$P_f = \Phi(-\beta)\,, \tag{22}$$

where Φ is the standard Gaussian CDF.

In this example, only beams in the reference standard test setup, as defined in Eq. (18), were considered. Consequently, the beam depth d can be used as the sole variable determining the beam size. The ultimate limit state, aligning with EN 1990 [43], aims to balance the characteristic values for the load effect S_k (mean value) and the resistance R_k (5th percentile)

$$\gamma_F\, S_k(d) = \frac{R_k(d)}{\gamma_M(d)}\,, \tag{23}$$

where γ_F and γ_M are partial safety factors applied to the load effect and resistance, respectively.

The focus is now on maintaining a constant reliability, thus a constant β can be prescribed by combining Eqs. (21) and (22). Specifying a constant β and a size-dependent probability distribution for the resistance P_R, the load effect p_S can be defined for a two-parameter probability distribution by knowing the type and CV. A constant β in the limit state is then maintained by linking Eqs. (21) to (23) and deriving the characteristic values from P_R and p_S. In this example, γ_F is constant. Based on these relationships, $\gamma_M(d)$ can be utilized to compensate for the size dependency of the resistance CV while maintaining a constant β.

To account for size dependency of the resistance while keeping β constant, the effects due to the varying characteristic resistance (i.e., strength) and its varying CV are considered separately. First, the effect of a varying characteristic strength is expressed for by the size modification factor

$$k_h(d) = \frac{R_k(d)}{R_{k,ref}}\,, \tag{24}$$

where $R_{k,ref}$ ($= f_{b,ref}$) is the characteristic reference resistance for the reference beam size in Eq. (17). Second, the effect of a varying resistance CV is included in the resistance-related partial safety factor

$$\gamma_M(d) = \frac{k_h(d)\, R_{k,ref}}{\gamma_F\, S_k(d)} \tag{25}$$

by using Eq. (24) in Eq. (23) and solving for $\gamma_M(d)$. The change in $\gamma_M(d)$ relative to a fixed reference partial safety factor $\gamma_{M,ref}$ is expressed by the partial-safety modification factor

$$k_\gamma(d) = \frac{\gamma_M(d)}{\gamma_{M,ref}}\,. \tag{26}$$

The modification factors from Eqs. (24) and (26) can be implemented on the resistance side of the ultimate limit state equation (23) to account for size dependency

$$\gamma_F\, S_k(d) = \frac{k_h(d)\, R_{k,ref}}{k_\gamma(d)\, \gamma_{M,ref}}\,. \tag{27}$$

Finally, this enables using the effective size modification factor

$$k_{h,eff}(d) = \frac{k_h(d)}{k_\gamma(d)} \tag{28}$$

to combine both effects while ensuring a constant β regardless of the structures' size.

5.2. Example with constant reliability

The example focuses on two objectives: first, a comparison of the results obtained using the log-normal and Weibull-Gaussian distributions; second, the sensitivity of the Weibull modulus m in the Weibull-Gaussian distribution. Both scenarios cover beam depths ranging from 160 mm to 3000 mm. The sensitivity is demonstrated using parameter Set 4, where m is reduced by 15% compared to Set 3 in Table 3. The adjustment of m requires recalibration of the CV of a single RVE ω_0 and the scale parameter s_0, as described in Section 3.1. The parameters in Set 4 are: $m = 24.1$, $s_0 = 1.331\,f_{\mathrm{b,ref}}$, and $\omega_0 = 0.1734$ with values of P_{gr} and V_{RVE} remaining identical to those in Set 3.

The load effect S was considered as a dead load following a Gaussian distribution with a CV $\omega_S = 0.1$, as recommended by JCSS [44]. Two different distribution types were analyzed for the size-dependent resistance R: the bending strength followed either a log-normal distribution consistent with the trends shown in Fig. 9 or a Weibull-Gaussian distribution using parameters from Set 3 or Set 4. Set 3 represented the optimal model parameters (Table 3), and Set 4 demonstrated the sensitivity of the Weibull modulus m. The partial safety factor for the dead load was set at $\gamma_{\mathrm{F}} = 1.35$ in accordance with EN 1990 [43].

The reliability index was $\beta = 4.4214$, matching the value obtained when using a log-normal distribution with a CV $\omega_f = 0.15$ as recommended by JCSS [28] and a partial safety factor $\gamma_{\mathrm{M}} = 1.25$ according to prEN 1995-1-1 [11]. This selection of β allows to relate the results to the design standard in [11]. For context, consequence class (CC) 3 with a 50-year reference period has a $\beta_{50} = 4.3$, as stated by EN 1990 [43]. This example considers only dead loads, while Köhler et al. [45] demonstrated the influence on β for GLT beams using dead and variable loads with different ratios.

In the design standard prEN 1995-1-1 [11], the resistance-related partial safety factor is constant at $\gamma_{\mathrm{M,ref}} = 1.25$. In this work, $\gamma_{\mathrm{M,ref}}$ is used as a reference for the partial-safety modification factor in Eq. (26). An equivalent to the size modification factor from Eq. (24) is provided by the depth modification factor

$$k_{\mathrm{h,prEN}} = \min\left\{\left(\frac{600}{d}\right)^{0.08}; 1.1\right\}, \tag{29}$$

where d is the beam depth in mm. The modification factors $k_{\mathrm{h,prEN}}$ and k_{h}, from Eqs. (24) and (29), respectively, both describe the change of the 5th percentile.

The predicted 5th percentiles of the log-normal and Weibull-Gaussian distributions deviated by a maximum of 3.5% within the analyzed size range, both using the parameters from Set 3. To demonstrate the sensitivity of the Weibull-Gaussian distribution regarding its parameters, the Weibull modulus m was reduced by 15% as an example. Reducing m required recalibrating s_0 and ω_0 with the modified parameters summarized in Set 4 at the beginning of this section. Using the Weibull-Gaussian distributions with parameters from Set 3 and 4 resulted in a deviation of the characteristic (5th-percentile) strengths and the mean strengths, which was less than 2% across the analyzed size range.

Plotting the resistance-related partial safety factor $\gamma_{\mathrm{M}}(d)$ from Eq. (25) for varying beam depths d revealed the effect of a variable CV (Fig. 10a). Generally, γ_{M} decreased as d increases. However, with the Weibull-Gaussian distribution, $\gamma_{\mathrm{M}}(d)$ remained constant for beams with depths greater than $d \approx 1.1$ m using the parameters from Set 3. For beams with the reference size of $d = 0.6$ m, both the log-normal distribution and the Weibull-Gaussian distribution with parameters from Set 3 yielded $\gamma_{\mathrm{M}} \approx 1.17$. For beams with $d = 3$ m, γ_{M} varied significantly, ranging from 1.06 for the log-normal distribution to 1.20 for the Weibull-Gaussian distribution using the parameters with the reduced m from Set 4.

The influence of the decreasing bending strength and CV was captured by the effective size modification factor $k_{\mathrm{h,eff}}(d)$ from Eq. (28) for varying beam depths d (Fig. 10b). Generally, $k_{\mathrm{h,eff}}$ decreased as d increases. While the Weibull-Gaussian distributions showed a decreasing trend with increasing depth, the log-normal distribution almost converges to a constant value for beams larger than $d = 2$ m. At the reference beam size with $d = 0.6$ m, both the log-normal distribution and the Weibull-Gaussian distribution with parameters from Set 3 resulted in $k_{\mathrm{h,eff}} \approx 1.07$. The reduced m in Set 4 for the Weibull-Gaussian distribution resulted in $k_{\mathrm{h,eff}}(d = 0.6\,\mathrm{m}) = 1.03$.

5.3. Discussion on resistance distributions

This discussion focuses on comparing the results obtained by the log-normal distribution and the Weibull-Gaussian distribution with the parameters from Set 3 in Table 3. The trends of mean bending strength $\bar{f}_{\mathrm{b}}$ and CV ω_f for both distributions consist with the trends shown in Fig. 9.

The log-normal distribution was chosen for comparison because the tensile or bending strength of timber structures is assumed to follow it, as prescribed by EN 14358 [27] for estimating the 5th percentile and recommended by JCSS [28] for probabilistic models. This distribution provides only positive values, making it suitable for describing strength, and it arises from the central limit theorem using products of random variables [46]. However, Bažant and Le [30] argue that using the log-normal distribution implies that the ultimate strength is the product of contributions across the failure surface, which is mechanically impossible. Despite this, its common use makes the comparison highly relevant.

The use of these two different distributions slightly influences the decrease of their 5th percentile, known as the size effect described by Eq. (24). At the reference size of $d = 0.6$ m, both distributions were calibrated to ensure their characteristic (5th-percentile) strength matches the strength class with a CV $\omega_f = 0.114$, resulting in a mean value deviation of 3%. Following the same decreasing trend in mean value, the 5th-percentile strength from the log-normal distribution is about 3% lower than that from the Weibull-Gaussian distribution for large beams with $d = 3$ m. Thus, the characteristic strength decrease predicted by both distributions is approximately the same.

The lower γ_{M} compared to $\gamma_{\mathrm{M,ref}} = 1.25$ for the reference-sized beams results from the reduced CV $\omega_f = 0.114$, as opposed to the recommended $\omega_f = 0.15$ by JCSS [28] (Fig. 10a). This difference causes the vertical shift of the effective size modification factor $k_{\mathrm{h,eff}}$ compared to the depth modification factor $k_{\mathrm{h,prEN}} = 1.0$ at $d = 0.6$ m from prEN 1995-1-1 [11] (Fig. 10b). Nevertheless, the decreasing trend of the Weibull-Gaussian distribution for $k_{\mathrm{h,eff}}$ is similar to $k_{\mathrm{h,prEN}}$ for the considered beam depths up to 3 m.

The significantly differing trends of the log-normal and Weibull-Gaussian distribution for large beams (Fig. 10b) are caused by the steady decrease of γ_{M} for the log-normal distribution (Fig. 10a). The constant γ_{M} for the Weibull-Gaussian distribution after a certain beam size is attributed to the constant CV on both sides: the load effect (Gaussian distribution) and resistance (left tail follows a Weibull distribution). The 5th percentile is derived from the Weibull part of the distribution for beam depths greater than $d \approx 1.1$ m.[4]

The analysis is limited to variable depths with fixed length-to-depth ratios and a four-point bending test with the load applied at the third

[4] When the characteristic values are derived from distributions with constant CVs, γ_{M} from Eq. (25) remains constant. Both the Gaussian distribution for the load effect and the Weibull part of the Weibull-Gaussian distribution for the resistance have a constant CV. Their right and left distribution tails, both with constant CVs, govern the convolution integral in Eq. (21). Consequently, maintaining a constant probability of failure results in a constant γ_{M}, even as the strength decreases further with increasing size.

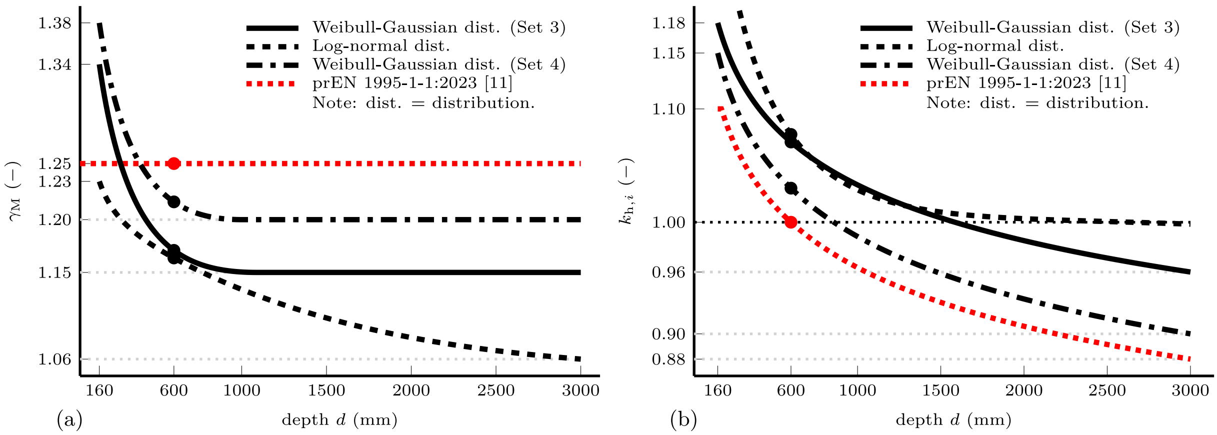

Fig. 10. Structural reliability analysis using Weibull-Gaussian and log-normal distributions with parameters from Set 3, as listed in Table 3, and Set 4, as provided at the beginning of Section 5.2, for variable beam depths d, focusing on (a) the partial safety factor $\gamma_M(d)$ and (b) the effective size modification factor $k_{h,eff}(d)$. For comparison, the current design specifications in prEN 1995-1-1 [11], which do not maintain constant structural reliability, are included, featuring a constant γ_M and the depth modification factor $k_{h,prEN}(d)$.

points. However, modern structures often have variable lengths for the same depth and different load configurations, such as distributed loads or off-centered three-point bending. These effects are important to consider in a comprehensive structural reliability analysis, which is feasible with the presented statistical mechanics-based model but beyond the scope of this study. This simple example showed that the Weibull-Gaussian distribution with parameters from Set 3 generally provides conservative results compared to the log-normal distribution with the same mean and CV.

5.4. Discussion on sensitivity

The parameter m solely defines the CV of the Weibull distribution, and the resistance-related partial safety factor $\gamma_M(d)$ heavily depends on this CV. Consequently, γ_M depends on m (Fig. 10a). Using parameters from Set 3 or Set 4, the depth beyond which γ_M remains constant varies (Fig. 10a). This variation arises from scaling the PDF based on the structure's size and load configuration, represented by the equivalent number of RVEs N_{eq}. Generally, the structure's size (volume V), at which γ_M becomes constant, depends on the stress distribution and model parameters m, P_{gr}, and V_{RVE}, as given in Eq. (4). In this example, the difference of depths beyond which γ_M remains constant were only caused by the modified m.

When comparing the results of the effective size modification factor $k_{h,eff}$ using the parameters from Set 3 and Set 4, a vertical shift becomes apparent, with the difference slightly increasing for beams with greater depths (Fig. 10b). In this case, the primary factor driving the vertical shift is the effect of γ_M. However, $k_{h,eff}$ also accounts for the effect of the characteristic strength reduction k_h, which contributes to the slight variation observed at larger beam depths. Theoretically, for sufficiently large structures where γ_M has already reached a constant value, the strength reduction depends solely on the Weibull modulus m, as discussed by Tapia and Aicher [25, Fig. 12].

The demonstrated dependency of the model parameters highlights the importance of accurate parameter identification and should motivate further research focusing on the Weibull part of the Weibull-Gaussian distribution. Additionally, a comprehensive sensitivity study of the parameters would be useful, as the grafting point probability is also expected to have a strong influence. These topics, however, were beyond the scope of this study.

6. Conclusions and outlook

The finite weakest-link theory can be used to formulate the PDFs of homogeneous GLT beams of different sizes, load configurations, and strength classes. The present work identifies all five model parameters: the Weibull modulus m, the scale parameter s_0, the grafting point probability P_{gr}, the CV of a single RVE ω_0, and the RVE volume V_{RVE}. These parameters were initially obtained by maximum likelihood estimations using numerical simulations [15] of beam sections in seven different sizes and two strength classes. Subsequently, ω_0 was tuned based on an experimental study [3] and s_0 was related to European strength classes [12]. General conclusions using the finite weakest-link theory framework are as follows:

- The statistical mechanics-based model successfully predicts the mean bending strength $\bar{f}_b$ and CV ω_f from experimental studies covering different beam sizes, load configurations, and strength classes over the last 38 years. For $\bar{f}_b$, all 40 experimental sets from nine studies result in a mean relative error of −0.1%. Given to the high sensitivity of ω_f to sample size, selecting 17 sets with sample sizes ≥ 10 from six studies yields a mean relative error of −1%.
- The model successfully accounts for different strength classes, as demonstrated by a linear regression between experimental and predicted $\bar{f}_b$ with an intercept close to zero and a slope of 1.03. The coefficient of determination is $R^2 = 0.818$. ω_f is considered independent of the strength class.

Regarding the dependency on beam size and load configuration, the following conclusions are drawn:

- The predicted PDFs provide specific pairings of $\bar{f}_b$ and ω_f. For reference-sized beams tested in the reference setup, both specified in Eqs. (17) and (18), the modeled 5th percentile corresponds to the characteristic strength $f_{b,ref}$ specified by European strength classes [12]. This configuration results in $\bar{f}_b = 1.25\, f_{b,ref}$ and $\omega_f = 0.114$. In contrast, JCSS [28] recommends a log-normal distribution with a higher CV of 0.15 for GLT beams, which leads to a similar $\bar{f}_b = 1.29, f b, ref$. Notably, the predicted ω_f deviates by only about 2% from the mean CV of experimentally tested beams of similar size and test setups.
- The trends of $\bar{f}_b$ and ω_f decrease with increasing tensile stressed volume. The obtained trends align with the results presented in a simulation study by Frese and Blaß [14]. However, the ω_f values presented in this study are consistently lower, showing an almost constant difference across the modeled size range. The beams in both studies were subjected to the reference test setup from Eq. (18), with depths up to 3.0 m. Unfortunately, the literature lacks experimental data of GLT beams larger than the reference size with sufficiently large sample sizes.
- The model successfully predicts the characteristic (5th-percentile) bending and tensile strength of homogeneous GLT beams in accordance with EN 14080 [12], using their reference size and test

setup as provided in EN 408 [32]. In [12], the tensile-to-bending strength ratio is 0.80, which agrees well with the predicted ratio of 0.84; in both cases, the ratio is independent of the strength class. However, further experimental data with different load configurations is necessary for validation.

Regarding the structural reliability demonstration, the following conclusions are drawn:

- Applying either a Weibull-Gaussian or log-normal distribution with the same decreasing $\bar{f}_\mathrm{b}$ and ω_f leads to significantly different trends in the effective size modification factor $k_\mathrm{h,eff}$ to ensure a constant reliability index β. Currently, the latter distribution is used for describing the bending and tensile strength of GLT beams in accordance with EN 14358 [27] and JCSS [28], though Bažant and Le [30] argue against its mechanical validity. Generally, the Weibull-Gaussian distribution yielded conservative results compared to those from the log-normal distribution.
- The parameters of the Weibull part of the Weibull-Gaussian distribution are crucial in a structural reliability analysis as they govern low probabilities and influence β. The presented example demonstrates the significant influence of the Weibull modulus on the partial safety factor γ_M. This underscores the importance of accurate parameter identification and should motivate further research on the parameters of the Weibull part.

Future research should focus on validating Weibull distribution parameters, exploring different load configurations experimentally with sufficient sample sizes, and analyzing the model's parameter sensitivity. Identifying the Weibull modulus m and the grafting point probability P_gr, where the distribution transitions from Weibull to Gaussian, seems most promising with tensile tests, since the specimen size can be much smaller than in bending tests according to the finite weakest-link theory. Additionally, extending the model to GLT beams with combined layups or those made from different wood species would be of significant interest.

Modern structures often use beams with varying sizes and load configurations, which should be considered in the design process to ensure the desired structural reliability. The presented modeling of probability distribution functions for GLT beams of various sizes and load configurations is a valuable tool to account for diverse structural applications. By addressing the outlined future research, the model's applicability can be further enhanced, supporting the development of more comprehensive design strategies in timber engineering.

CRediT authorship contribution statement

Christoffer Vida: Writing – original draft, Visualization, Validation, Software, Methodology, Investigation, Formal analysis, Data curation, Conceptualization. **Markus Lukacevic:** Writing – review & editing, Supervision, Conceptualization. **Sebastian Pech:** Writing – review & editing, Supervision, Conceptualization. **Josef Füssl:** Writing – review & editing, Supervision, Funding acquisition, Conceptualization.

Declaration of competing interest

The authors declare that they have no known competing financial interests or personal relationships that could have appeared to influence the work reported in this paper.

Acknowledgments

This research was funded in whole, or in part, by the Austrian Science Fund (FWF)[Y1093–N30] and [F77]. For the purpose of open access, the author has applied a CC BY public copyright license to any Author Accepted Manuscript version arising from this submission. The authors acknowledge TU Wien Bibliothek for financial support through its Open Access Funding Program.

Appendix A. Classification of reference bending strength

This appendix relates the experimental studies conducted up to 1995 in Table 1 to the current strength classes in [12] or the reference bending strengths $f_\mathrm{b,ref}$. $f_\mathrm{b,ref}$ represents the 5th-percentile strength for beams of the reference size specified in Eq. (17) tested in the reference setup from Eq. (18). In some studies, the reference size and load configuration differed, requiring adjustments.

To account for different beam sizes and load configurations, the model presented herein was applied with parameters from Set 3 in Table 3. The 5th-percentile bending strength $f_\mathrm{b,05}$, corresponding to a specific beam size and load configurations, can be converted to $f_\mathrm{b,ref}$ by applying the ratio

$$k = \frac{f_\mathrm{b,ref}}{f_\mathrm{b,05}}\,. \tag{A.1}$$

The ratio k is independent of the strength class and thus is $f_\mathrm{b,ref}$. $f_\mathrm{b,05}$ was calculated for its specific beam size and load configuration based on the PDF obtained by the present model.

A.1. Ehlbeck and Colling [1]

The tested GLT beams reported by Ehlbeck and Colling [1] consisted of laminations from strength class GK II and GK I according to DIN 4074-1:1958 [47]. The beams were mainly manufactured homogeneously from GK II. However, individual sets included a single beam using the higher strength class GK I for the outermost lamination (Table 1). A weak trend of an increased bending strength was reported for the beams using the higher strength class in the outermost lamination, but due to the small sample size, the increase was inconclusive.

Nowadays, beams manufactured from laminations of strength class GK II correspond to strength class GL24h according to EN 14080 [12]. This classification was made by using DIN 1052-1 [48] and DIN 1052-1 [49] to first assign the beams to the former strength class BS11, and then applying DIN 1052 [50] to link the former and current strength classes.

A.2. Colling [2]

Experimental tests presented by Colling [2] consisted of GLT beams manufactured from laminations graded by varying strength grading criteria. All beams were loaded in four-point bending. Additionally, Colling [2] introduce a model that was used to predict the characteristic bending strength of the tested beams. A systematic underestimation of their characteristic bending strength is stated in [2]. In comparison to the reference beam size, the beams were shorter and thinner. Herein, we used the predictions provided in [2] and account for the different size and load configuration by $k = 0.9283$.

A.3. Falk et al. [3]

The study conducted by Falk et al. [3] used the strength classes LH35 and LH40, where the digits are dedicated to the characteristic bending strengths of beams having a depth of 300 mm. Thus, we herein applied $k = 0.8521$ to translate their strength classes to the reference beam size and load configuration.

A.4. Aasheim and Solli [4]

Boards corresponding to the Norwegian strength class T30 were used to manufacture the GLT beams in the study presented by Aasheim and Solli [4]. Additionally, 15 finger joints were tested to determine their tensile strength. With their characteristic board bending strength of $30\,\mathrm{N\,mm^{-2}}$ and the reported characteristic finger-joint tensile strength of about $27\,\mathrm{N\,mm^{-2}}$, we assigned the beams to the strength class GL28h according to EN 14080 [12].

A.5. Gehri et al. [5]

Gehri et al. [5] tested GLT beams built from machine graded boards resulting in the strength classes MS10h, MS13h, and MS17h. The reported tensile strength, tensile modulus of elasticity, and density enabled us to assign the strength classes GL20h, GL26h and GL30h according to EN 14080 [12]. Additionally, the reported finger-joint bending strengths fulfilled these assignments.

Appendix B. Calculation of mean bending strength and standard deviation

First, the calculation of the mean bending strength $\bar{f}_\mathrm{b}$ and standard deviation δ_f is presented for the experimental results, followed by the model predictions. For experimentally obtained bending strengths f_b, the estimate of $\bar{f}_\mathrm{b}$ was

$$\bar{f}_\mathrm{b} = \frac{1}{n}\sum_{i=1}^{n} f_{\mathrm{b},i}\,, \tag{B.1}$$

and the standard deviation was defined by

$$\delta_f = \left[\frac{1}{n-1}\sum_{i=1}^{n}\left(f_{\mathrm{b},i} - \bar{f}_\mathrm{b}\right)^2\right]^{1/2}. \tag{B.2}$$

Most experimental studies [1,2,8–10] report individual results, for which Eqs. (B.1) and (B.2) were used. For the study by Falk et al. [3], individual results were extracted from a figure in their report. The studies by Aasheim and Solli [4], Gehri et al. [5], Brandner et al. [7] provided mean and CV values, which were used directly.

For the model predictions, the present model was employed. The probability density distribution $p_f(x)$, which is the derivative of Eq. (3) with respect to x, was used to calculate

$$\bar{f}_\mathrm{b} = \int_0^\infty x\, p_f(x)\,\mathrm{d}x\,, \tag{B.3}$$

and

$$\delta_f = \left[\int_0^\infty \left(x - \bar{f}_\mathrm{b}\right)^2 p_f(x)\,\mathrm{d}x\right]^{1/2}, \tag{B.4}$$

where x denotes the bending strength f_b described by the distribution.

Data availability

Data will be made available on request.

References

[1] J. Ehlbeck, F. Colling, Biegefestigkeit von Brettschichtholz in Abhängigkeit von Rohdichte, Elastizitätsmodul, Ästigkeit und Keilzinkung der Lamellen, der Lage der Keilzinkung sowie von der Trägerhöhe. Teil A: Karlsruher Untersuchung, Forschungsbericht der Versuchsanstalt für Stahl, Holz und Steine, Ingenieurholzbau, Universität Karlsruhe, Karlsruhe, Germany, 1987.

[2] F. Colling, Tragfähigkeit von Biegeträgern aus Brettschichtholz in Abhängigkeit von den Festigkeitsrelevanten Einflussgrößen (Ph.D. thesis), Universität Karlsruhe, Karlsruhe, Germany, 1990.

[3] R.H. Falk, K.H. Solli, E. Aasheim, The performance of glued laminated beams manufactured from machine stress graded Norwegian spruce, in: Meddelelse 77, Norsk Treteknisk Institutt, Oslo, 1992.

[4] E. Aasheim, K.H. Solli, Size factor of Norwegian glued laminated beams, in: Proc. 28th CIB-W18 Meet. CIB-W/28-12-2, Copenhagen, Denmark, 1995.

[5] E. Gehri, S. Koller, R. Mauritz, K. Palm, R. Pischl, G. Schickhofer, C. Seiner, A. Steinberger, P. Wörle, Entwicklung leistungsfähiger Holzleimbauteile durch den Einsatz von maschinell festigkeitssortiertem Holz, Tagungsband zur Präsentation des FFF-Forschungsprojektes, Graz, Austria, 1995.

[6] G. Schickhofer, Development of efficient glued laminated timber, in: Proc. 29th CIB-W18 Meet. CIB-W18/29-12-1, Bordeaux, France, 1996.

[7] R. Brandner, B. Freytag, G. Schickhofer, Determination of shear modulus by means of standardized four-point bending tests, in: Proc. 41st CIB-W18 Meet. CIB-W18/41-21-1, St. Andrews, Canada, 2008.

[8] G. Fink, A. Frangi, J. Kohler, Bending tests on GLT beams having well-known local material properties, Mater. Struct. 48 (2015) 3571–3584, http://dx.doi.org/10.1617/s11527-014-0424-2.

[9] G. Kandler, M. Lukacevic, J. Füssl, Experimental study on glued laminated timber beams with well-known knot morphology, Eur. J. Wood Wood Prod. 76 (2018) 1435–1452, http://dx.doi.org/10.1007/s00107-018-1328-6.

[10] G. Fink, P. Stadelmann, A. Frangi, Bending test on large-scale GLT beams with well-known beam setup using machine grading indicator, Int. Wood Prod. J. 12 (2021) 258–266, http://dx.doi.org/10.1080/20426445.2021.1969166.

[11] prEN 1995-1-1:2023, Eurocode 5 – Design of Timber Structures – Part 1-1: General Rules and Rules for Buildings, European Standard, European Committee for Standardization, Brussels, Belgium, 2023.

[12] EN 14080:2013, Timber Structures – Glued Laminated Timber and Glued Solid Timber – Requirements, European Standard, European Committee for Standardization, Brussels, Belgium, 2013.

[13] G. Fink, A. Frangi, J. Kohler, Probabilistic approach for modelling the load-bearing capacity of glued laminated timber, Eng. Struct. 100 (2015) 751–762, http://dx.doi.org/10.1016/j.engstruct.2015.06.015.

[14] M. Frese, H.J. Blaß, Reliability of large glulam members part 1: Data for the assessment of partial safety factors for the bending strength, in: Proc. 49th INTER Meet. INTER/49-17-1, Graz, Austria, 2016.

[15] C. Vida, M. Lukacevic, G. Hochreiner, J. Füssl, Size effect on bending strength of glued laminated timber predicted by a numerical simulation concept including discrete cracking, Mater. Des. 225 (2023) 111550, http://dx.doi.org/10.1016/j.matdes.2022.111550.

[16] G. Fink, R. Brandner, P. Palma, J. Kohler, Volume effects in glued laminated timber beams, in: Proc. 14th ICASP, Dublin, Ireland, 2023.

[17] W. Weibull, A statistical theory of the strength of materials, Handlingar Nr. 151, Ingeniörsvetenskapsakademiens, Generalstabens Litografiska Anstalts Förlag, Stockholm, Sweden, 1939.

[18] B. Bohannan, Effect of size on bending strength of wood members, Research Paper FPL-56, U.S. Department of Agriculture, Forest Service, Forest Products Laboratory, Madison, Wisconsin, USA, 1966.

[19] S. Schilling, P. Palma, R. Steiger, A. Frangi, Probabilistic description of the mechanical properties of glued laminated timber made from softwood, in: Proc. 54th INTER Meet. INTER/54-12-4, 2021, online.

[20] Z.P. Bažant, Probability distribution of energetic-statistical size effect in quasibrittle fracture, Probabilistic Eng. Mech. 19 (2004) 307–319, http://dx.doi.org/10.1016/j.probengmech.2003.09.003.

[21] Z.P. Bažant, S.-D. Pang, Mechanics-based statistics of failure risk of quasibrittle structures and size effect on safety factors, Proc. Natl. Acad. Sci. 103 (2006) 9434–9439, http://dx.doi.org/10.1073/pnas.0602684103.

[22] Z.P. Bažant, S.-D. Pang, Activation energy based extreme value statistics and size effect in brittle and quasibrittle fracture, J. Mech. Phys. Solids 55 (2007) 91–131, http://dx.doi.org/10.1016/j.jmps.2006.05.007.

[23] S.-D. Pang, Z.P. Bažant, J.-L. Le, Statistics of strength of ceramics: Finite weakest-link model and necessity of zero threshold, Int. J. Fract. 154 (2008) 131–145, http://dx.doi.org/10.1007/s10704-009-9317-8.

[24] J.-L. Le, A. Cannone Falchetto, M.O. Marasteanu, Determination of strength distribution of quasibrittle structures from mean size effect analysis, Mech. Mater. 66 (2013) 79–87, http://dx.doi.org/10.1016/j.mechmat.2013.07.003.

[25] C. Tapia, S. Aicher, Survival analysis of tensile strength variation and simulated length–size effect along oak boards, J. Eng. Mech. 148 (2022a) 04021130, http://dx.doi.org/10.1061/(ASCE)EM.1943-7889.0002006.

[26] C. Tapia, S. Aicher, Size effect of glulam made of oak wood under consideration of the finite weakest link theory, in: Proc. 55th INTER Meet. INTER/55-12-2, Bad Aibling, Germany, 2022b.

[27] EN 14358:2016, Timber Structures – Calculation and Verification of Characteristic Values, European Standard, European Committee for Standardization, Brussels, Belgium, 2016.

[28] JCSS, Probabilistic Model Code – Part 3: Resistance Models (3.05 Timber), 2006.

[29] J.-L. Le, Z.P. Bažant, M.Z. Bazant, Unified nano-mechanics based probabilistic theory of quasibrittle and brittle structures: I. Strength, static crack growth, lifetime and scaling, J. Mech. Phys. Solids 59 (2011) 1291–1321, http://dx.doi.org/10.1016/j.jmps.2011.03.002.

[30] Z.P. Bažant, J.-L. Le, Probabilistic Mechanics of Quasibrittle Structures: Strength, Lifetime, and Size Effect, Cambridge University Press, Cambridge, UK, 2017, http://dx.doi.org/10.1017/9781316585146.

[31] J.-L. Le, Z. Xu, J. Eliáš, Internal length scale of weakest-link statistical model for quasi-brittle fracture, J. Eng. Mech. 144 (2018) 04018017, http://dx.doi.org/10.1061/(ASCE)EM.1943-7889.0001430.

[32] EN 408:2010+A1:2012, Timber Structures – Structural Timber and Glued Laminated Timber – Determination of Some Physical and Mechanical Properties, European Standard, European Committee for Standardization, Brussels, Belgium, 2012.

[33] A. Hazen, Storage to be provided in impounding municipal water supply, Trans. Am. Soc. Civ. Eng. 77 (1914) 1539–1640, http://dx.doi.org/10.1061/taceat.0002563.

[34] Abaqus, Abaqus 2021 HF5, Software, Dassault Systèmes Simulia Corp., Providence, RI, USA, 2021.

[35] M. Lukacevic, J. Füssl, R. Lampert, Failure mechanisms of clear wood identified at wood cell level by an approach based on the extended finite element method, Eng. Fract. Mech. 144 (2015) 158–175, http://dx.doi.org/10.1016/j.engfracmech.2015.06.066.

[36] M. Lukacevic, W. Lederer, J. Füssl, A microstructure-based multisurface failure criterion for the description of brittle and ductile failure mechanisms of clear-wood, Eng. Fract. Mech. 176 (2017) 83–99, http://dx.doi.org/10.1016/j.engfracmech.2017.02.020.
[37] S. Pech, M. Lukacevic, J. Füssl, A robust multisurface return-mapping algorithm and its implementation in Abaqus, Finite Elem. Anal. Des. 190 (2021) 103531, http://dx.doi.org/10.1016/j.finel.2021.103531.
[38] Z.P. Bažant, D. Novák, Energetic-statistical size effect in quasibrittle failure at crack initiation, ACI Mater. J. 97 (2000) http://dx.doi.org/10.14359/9879.
[39] ANSI/AWC NDS-2024, National Design Specification (NDS) for Wood Construction, National Standard in the USA, American Wood Council (AWC), Leesburg, VA, USA, 2024.
[40] Z.P. Bažant, I.M. Daniel, Z. Li, Size effect and fracture characteristics of composite laminates, J. Eng. Mater. Technol. 118 (1996) 317–324, http://dx.doi.org/10.1115/1.2806812.
[41] M. Frese, Y. Chen, H.J. Blaß, Tensile strength of spruce glulam, Eur. J. Wood Prod. 68 (2010) 257–265, http://dx.doi.org/10.1007/s00107-010-0449-3.
[42] R.E. Melchers, A.T. Beck, Structural Reliability Analysis and Prediction, 3rd ed., Wiley, Hoboken, NJ, USA, 2018.
[43] EN 1990:2023, Eurocode – Basis of Structural and Geotechnical Design, European Standard, European Committee for Standardization, Brussels, Belgium, 2023.
[44] JCSS, Probabilistic Model Code – Part 2: Load Models (2.01 Self Weight), 2001.
[45] J. Köhler, J.D. Sørensen, M. Baravalle, Calibration of existing semi-probabilistic design codes, in: Proc. 13th ICASP, 2019, http://dx.doi.org/10.22725/ICASP13.325.
[46] P.M. Shankar, Probability, Random Variables, and Data Analytics with Engineering Applications, Springer International Publishing, Cham, Switzerland, 2021, http://dx.doi.org/10.1007/978-3-030-56259-5.
[47] DIN 4074-1:1958, Bauholz für Holzbauteile; Gütebedingungen für Bauschnittholz (Nadelholz), German Standard, NormenausschußBauwesen im Deutschen Institut für Normung e.V., Berlin, Germany, 1958.
[48] DIN 1052-1:1988, Holzbauwerke; Berechnung und AusfÜhrung, German Standard, NormenausschußBauwesen im Deutschen Institut für Normung e.V., Berlin, Germany, 1988.
[49] DIN 1052-1/A1:1996-10, Holzbauwerke – Teil 1; Berechnung und Ausführung; Änderungen 1, German Standard, NormenausschußBauwesen im Deutschen Institut für Normung e.V., Berlin, Germany, 1996.
[50] DIN 1052:2008-12, Entwurf, Berechnung und Bemessung von Holzbauwerken – Allgemeine Bemessungsregeln und Bemessungsregeln für den Hochbau, German Standard, Normenausschuss Bauwesen im Deutschen Institut für Normung e.V., Berlin, Germany, 2008.